water

MDPI

Article

Spatiotemporal Patterns of Terrestrial Evapotranspiration in Response to Climate and Vegetation Coverage Changes across the Chinese Loess Plateau

Han Zheng [1,2,*], Henry Lin [3,*] and Xianjin Zhu [4]

1 Key Laboratory of Subsurface Hydrology and Ecological Effect in Arid Region of Ministry of Education, School of Environmental Science and Engineering, Chang'an University, Xi'an 710054, China
2 State Key Laboratory of Loess and Quaternary Geology, CAS Center for Excellence in Quaternary Science and Global Change, Institute of Earth Environment, Chinese Academy of Sciences, Xi'an 710061, China
3 Department of Ecosystem Science and Management, The Pennsylvania State University, University Park, PA 16802, USA
4 College of Agronomy, Shenyang Agricultural University, Shenyang 110161, China
* Correspondence: zhenghan@chd.edu.cn (H.Z.); henrylin@psu.edu (H.L.)

Received: 21 June 2019; Accepted: 5 August 2019; Published: 6 August 2019

Abstract: Spatiotemporal patterns of evapotranspiration (ET) and its controlling factors are important for ecosystem services and water resources management in the Chinese Loess Plateau (CLP). In this study, we assessed the spatial patterns of ET and then investigated the interannual variability of ET and its relationships with climate variability and vegetation coverage changes at the timescales of annual, active growing season, as well as different seasons across the entire CLP from 2000 to 2014. A MODIS-derived ET dataset, ground-based datasets of precipitation and atmospheric evaporative demand (AED), and a remote-sensing dataset of Normalized Difference Vegetation Index (NDVI) were comprehensively analyzed. Results showed that mean annual ET varied distinctly among different vegetation zones, generally higher in the more humid southeastern parts of the CLP. Summer ET and ET over active growing season significantly increased for more than 40% of the entire CLP area, and winter ET significantly decreased over ~70% of the entire CLP region, while annual ET, spring ET, and autumn ET remained quite stable during 2000–2014. Per-pixel interannual variability of ET was mainly positively correlated with that of precipitation and NDVI except for winter, but negatively correlated with AED trends. Our study also demonstrated that ET variation trends were exactly consistent for the entire CLP region, the areas mainly implemented with the Grain for Green (GFG) project, and other CLP areas not implemented with the GFG project during 2000–2014. Our findings suggest that the spatiotemporal patterns of CLP ET were mainly water-limited, and climate variability played an essential role in shaping the interannual variability of ET in the CLP. This study will improve our understanding on the ET variations over water-limited areas under climate and vegetation coverage changes.

Keywords: evapotranspiration; climate change; vegetation coverage change; interannual variability; Chinese Loess Plateau

1. Introduction

Ecosystem evapotranspiration (ET) is a key process and component in the terrestrial water cycle and energy balance [1,2], which is composed of vegetation transpiration, soil evaporation, and evaporation of canopy interception [2,3]. It has been reported that more than 60% of precipitation is returned to the atmosphere through the ET process at the global scale [4,5], and this ratio could be much higher for water-limited ecosystems [1,6]. Therefore, analyzing the spatiotemporal variation in

ET and its controlling factors is crucial for water resources management especially for the water-limited regions around the world [1,7,8].

The Chinese Loess Plateau (CLP) has long been threatened by soil erosion and environmental degradation [9,10]. Several revegetation or ecological restoration projects have been enforced in this region ever since the 1950s aiming at relieving the environmental pressure in the CLP, which have remarkably altered the land surface characteristics (e.g., increasing vegetation coverage) and ecosystem water cycles (e.g., declining runoff and soil moisture), particularly because of the implementation of the Grain for Green (GFG) project in 1999 [11–15]. The water resource limits for revegetation has also been reported in the CLP region [11]. As a key process within the water cycle, it is essential to comprehensively assess the spatiotemporal patterns of ecosystem ET for the water resources management across the CLP region.

Regional-scale ET variation has been studied mainly based on data synthetization of site-level observations [1,6], and ET models or algorithms combined with gridded inputs (e.g., satellite remote-sensing datasets) [16–19]. Site-level ET could be obtained with diverse observational or estimating methods [2], and the most commonly used method in the CLP region is the traditional water balance method (e.g., [20,21]), which generally pours all the uncertainties and measurement errors associated with water balance into the ET estimation [2,22]. The shortage in the data precision, as well as lack of temporal continuity and inter-site comparability in these ET data, have limited our understanding on the spatiotemporal variations in the CLP ET from an integrate perspective through synthesizing site-level ET observations. The fragmentized landforms in the CLP makes the site representativeness more complex [23]. Meanwhile, only very few sites have ever conducted ET observation with the eddy covariance method [23], a widely acceptable standard method for directly measuring ecosystem ET [24,25]. Therefore, current studies involving ET variations at the CLP-regional scale mainly depend on related model outputs and satellite datasets [11,13,23,26].

The spatiotemporal patterns of ecosystem ET in the CLP have been preliminarily analyzed mainly based on the MODerate Resolution Imaging Spectroradiometer (MODIS) ET product (MOD16), which records large-scale and long-term changes in terrestrial ET with a high spatial-temporal resolution [16,27]. The spatial pattern of annual ET has been indicated to be consistent with the gradients of precipitation and vegetation coverage [26,28]. As to the temporal variations in ET, previous studies have indicated that annual ET derived from the MODIS ET dataset has increased in the whole CLP region and its revegetated areas during 2000–2010 [11,23,26], and Feng et al. [11] attribute this increase to the land-use change rather than climate change in the CLP. However, it is still not clearly known yet how the ET variation responds to the climate change and vegetation coverage change in the CLP, whether the CLP ET is water-limited or energy-limited, and what the dominant factors are in affecting the interannual variability of ET at different timescales. The temporal variations in ET and influencing factors (e.g., net radiation, air temperature, and vapor pressure deficit) within short periods (e.g., daily and seasonal) have been well studied, but our knowledge on the interannual variability of ecosystem ET is still limited, which is of great importance for a deeper understanding of ecosystem water consumption in the CLP for sustainable development, especially under the influence of large regional-scale revegetation efforts and global climate change.

This research aimed at investigating the spatiotemporal patterns in the ecosystem ET and its relationships with climate variability and vegetation coverage changes across the Chinese Loess Plateau over the period since the first year after the large-scale implementation of the GFG project in 2000 until recently in 2014. A MODIS ET dataset, ground-based datasets of precipitation and atmospheric evaporative demand (AED), and a remote sensing-based dataset of Normalized Difference Vegetation Index (NDVI) were mainly applied. To achieve this, three research contents were proposed: (1) assessing the spatial distributions of ecosystem ET among different vegetation zones across the entire CLP; (2) analyzing the interannual variability of ET at the timescales of annual, active growing season, and different seasons (i.e., spring, summer, autumn, and winter) during 2000–2014; and (3) evaluating the relationships of ET trends with the trends in precipitation, AED, and NDVI at different timescales.

2. Data and Methods

2.1. Study Area

This study was conducted across the entire CLP area in the northwest of China. The CLP region covers an area of approximately 640,000 km^2 (34–40° N, 102–114° E, Figure 1a), generally showing higher elevation in the west and lower elevation in the east (Figure 1a). The CLP area is located in the temperate continental monsoon climatic zone, and experiences hot and wet summers, and cold and dry winters due to the effect of the Siberian high weather system and Asian monsoon [9,29]. The mean annual precipitation in the CLP increases from 130 mm to 815 mm, and the mean annual air temperature varied within the interval of about 3–15 °C during 2000–2014 (Figure 1b,c). The vegetation distribution patterns are strongly controlled by the northwest–southeast precipitation gradient, with forest and forest-steppe mainly in the southeast (Figure 1a) [9].

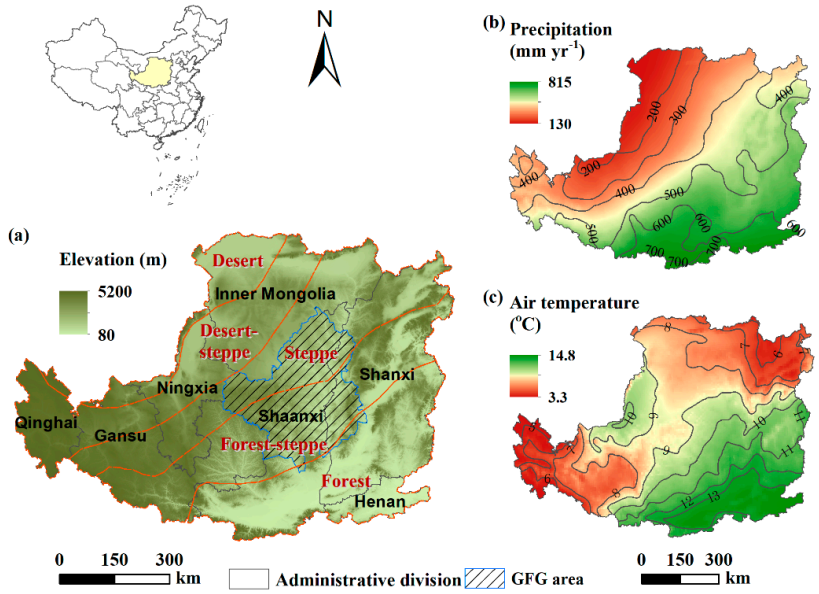

Figure 1. (**a**) Location and elevation of the Chinese Loess Plateau (CLP). Grey lines represent boundaries of administrative divisions in this region. Orange lines represent boundaries of five vegetation zones. Blue polygon with black slashes represents the main areas implemented with the Grain for Green (GFG) project in the CLP [10]. (**b**,**c**) Spatial distributions of (**b**) annual precipitation and (**c**) annual mean air temperature in the CLP averaged over 2000–2014. The gray lines in panel (**b**) and (**c**) are the isolines of precipitation and air temperature, respectively.

2.2. MODIS ET Dataset

We acquired monthly and annual ET data from the MODIS Collection 5 ET data product (MOD16 A2/A3), both with a spatial resolution of 1 km^2 during the time period from 2000 to 2014. This global terrestrial ET data product (MOD16) has been widely employed to ET and related researches at various space–time scales in the CLP and other regions in the world (e.g., [11,17]). The MODIS ET algorithm is based on the Penman–Monteith equation using gridded meteorological reanalysis dataset from NASA's Global Modeling and Assimilation Office (GMAO) and remote sensing data products from other MODIS data products as inputs [16,27].

The MODIS ET algorithm has been proved to show good performance in generating monthly and annual ET observations measured by open-path or close-path eddy covariance systems in the CLP and China (R^2 = 0.6, Figures S1 and S2). These ET observations were provided by a site-level ET dataset in China, which was constructed by synthesizing eddy-covariance ET data from ChinaFLUX and published literature in China [1,30]. Since there are very few eddy-covariance sites distributed in the CLP region, we first validated the performance of MODIS ET in capturing ET variations in

China with the yearly ET records in the site-level ET dataset, that is 149 site-year records of annual ET from 45 ecosystems (green diamonds shown in Figure S1). Then, 99 monthly ET data from five sites in the CLP (black flags shown in Figure S1) were used to validate the performance of MODIS ET in generating monthly ET data in the CLP.

We then calculated ET values over the active growing season as the sum of monthly ET data from April to September in each year at the pixel scale. The ET amounts in different seasons were also calculated for each year during 2000–2014, i.e., spring (from March to May), summer (from June to August), autumn (from September to November), and winter (from December to February in the following year).

2.3. Datasets of Precipitaion and NDVI

The relationships between the interannual variabilities of ET and precipitation (P), atmospheric evaporative demand (AED), and NDVI were analyzed. We first acquired the monthly datasets of P, air temperature (T_a), and actual vapor pressure (e_a) during 2000–2014 from approximately 756 meteorological stations in China. The AUSPLIN software was then utilized to produce the corresponding monthly gridded datasets of P, T_a, and e_a across the whole China region with a 1 km^2 spatial resolution using the method of thin-plate smoothing splines, which takes a digital elevation model as a third independent variable [1,31]. The performance of these gridded P and T_a datasets was validated using ~150 site-year records of point-scale measurements of annual total P and annual mean T_a from 62 sites in China (diamonds shown in Figure S1), which were obtained from the auxiliary P and T_a data of the site-level ET dataset introduced above. None of the 62 sites repeat with the 756 meteorological stations used for producing gridded P and T_a dataset. Good performance has been demonstrated, with R^2 both of 0.91 and root mean square error (RMSE) of 146.5 mm yr^{-1} and 1.94 °C for P and T_a dataset, respectively (Figures S1 and S3). Then, the gridded datasets of P, T_a, and e_a over the CLP area were extracted from the corresponding gridded datasets during the study period. Per-pixel annual P was computed as the sum of 12 monthly precipitation data for one year. The p-values over an active growing season as well as different seasons were also computed in this way. The monthly datasets of T_a and e_a were used to calculated AED introduced below.

As a critical remote-sensing indicator for vegetation growth, NDVI was selected to represent vegetation coverage in this study. We obtained the monthly NDVI data from a MODIS dataset with a spatial resolution of 1 km^2. The annual mean NDVI was computed as the mean of 12 NDVI data during one year at the pixel scale. The mean NDVI values for active growing season and different seasons were also calculated.

2.4. Calculation of Atmospheric Evaporative Demand

The AED variation can be quantized using pan evaporation, reference evapotranspiration, and potential evapotranspiration (PET), in which PET is an important measure representing AED of actual land surfaces under given metrological conditions [32]. It has been proved that the Linacre model [33], one of the numerous PET models, could faithfully reproduce AED dynamics for both the energy- and water-limited conditions [32]. Thus, the Linacre model was used in this study to calculate monthly AED values (mm month^{-1}, Equation (1)):

$$AED = \frac{\frac{500(T_a+0.006z)}{100-A} + 15(T_a - T_d)}{80 - T_a} \times J \quad (1)$$

where T_a is monthly mean air temperature (°C), z is elevation above sea level (m), A is latitude (degrees), T_d is dewpoint temperature (°C), J is the number of the day in a month. T_d is calculated using actual vapor pressure according to Reference [34]. The monthly gridded datasets of T_a, e_a, and z were used to generate gridded data of monthly AED. The AED values over active growing season and different seasons were then computed.

2.5. Data Analysis

In this study, we analyzed the spatial patterns of annual ET, *P*, AED, NDVI, as well as the ratio of ET over active growing season to annual ET (denoted as AGS-ET/Annual ET ratio hereafter), and ET amounts in different seasons by averaging the corresponding datasets during 2000–2014 at the pixel scale. Their mean annual values were then calculated for diverse vegetation zones (i.e., forest, forest-steppe, steppe, desert-steppe, and desert, Figure 1a). Only pixels with mean annual NDVI values larger than 0.1 were involved in this study.

The interannual variation in the CLP ET was assessed by calculating the linear slope values of ET values for the timescales of annual, active growing season, as well as different seasons during the study period on a per pixel basis. The interannual trends were statistically significant if p-values < 0.05. Time series with missing values were excluded from the temporal trend analysis in this study. We also examined the spatial-average interannual variabilities of ET, *P*, AED, and NDVI at different timescales by averaging all the pixels in the CLP. The temporal variations in ET were also analyzed for the main areas implemented with the GFG project and other CLP areas not implemented with the GFG project.

The relationships of ET trends with the interannual trends of *P*, AED, and NDVI were evaluated using the Pearson's correlation analyses at the timescales of annual, active growing season, and different seasons under a per-pixel basis. In addition, we performed detrended calculation to the time series in this study in consideration of the possible spurious correlations between two variables with same variation tendency [23].

3. Results

3.1. Spatial Pattern of ET in the CLP

Mean annual ET varied distinctly among different vegetation zones across the CLP region, with the overall spatial average of 347.8 ± 131.5 mm yr^{-1}, and generally showing higher values in the forest and forest-steppe zones than other zones (Figure 2a and Table 1). Similar spatial patterns were also observed in the spring ET, summer ET, and autumn ET in the CLP, while the differences in winter ET were relatively small among different zones in the CLP (Figure 3). The spatial patterns of AGS-ET/Annual ET ratio, precipitation, and NDVI were similar with that of ET, that is, generally higher for the more humid southeastern areas than in the arid and semi-arid areas (Figures 1b and 2b,c, Table 1). The spatial distribution of AED varied differently from that of ET, showing consistently higher AED values for the arid and semi-arid areas (Figure 2d).

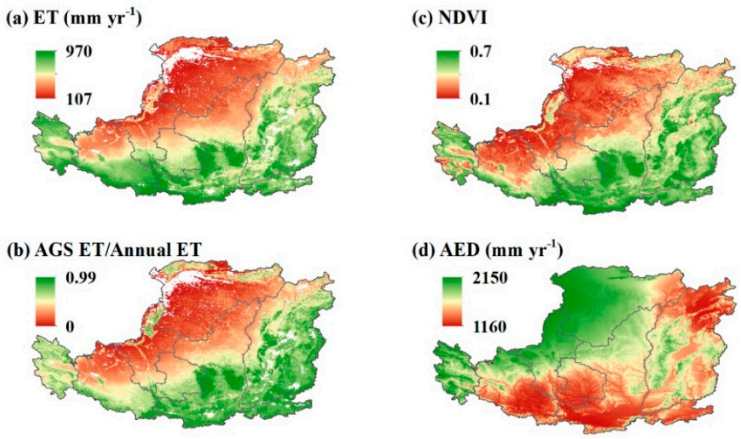

Figure 2. Spatial patterns of (**a**) mean annual evapotranspiration (ET), (**b**) the ratio of ET over active growing season to annual ET (AGS-ET/Annual ET ratio), (**c**) mean annual Normalized Difference Vegetation Index (NDVI), and (**d**) mean annual atmospheric evaporative demand (AED) averaged over 2000–2014 in the Chinese Loess Plateau.

Table 1. Statistical characteristics of ET and AGS-ET/Annual ET ratio for different vegetation zones averaged over 2000–2014 in the Chinese Loess Plateau. The *P*, AED, and NDVI values are also provided for reference. Different superscript letters denote a statistically significant difference at a 5% confident level based on Tukey's multiple comparison tests.

Vegetation Zone	ET (mm yr^{-1})	AGS-ET/Annual ET Ratio	*P* (mm yr^{-1})	AED (mm yr^{-1})	NDVI
Forest	328.6 ± 86.9 ^{a}	0.7 ± 0.05 ^{a}	576.1 ± 56.9 ^{a}	1406.2 ± 81.5 ^{e}	0.43 ± 0.09 ^{a}
Forest-steppe	272.9 ± 99.5 ^{b}	0.63 ± 0.07 ^{b}	500.1 ± 35.9 ^{b}	1412.1 ± 78.8 ^{d}	0.37 ± 0.1 ^{b}
Steppe	142.6 ± 58.7 ^{c}	0.5 ± 0.07 ^{c}	395.3 ± 41.7 ^{c}	1455.5 ± 86.1 ^{c}	0.23 ± 0.06 ^{c}
Desert-steppe	134.7 ± 90 ^{d}	0.46 ± 0.12 ^{d}	299 ± 63.9 ^{d}	1603.9 ± 73.2 ^{b}	0.21 ± 0.09 ^{d}
Desert	99.8 ± 70.4 ^{e}	0.43 ± 0.13 ^{e}	205.1 ± 46.8 ^{e}	1680 ± 70.4 ^{a}	0.18 ± 0.08 ^{e}
Mean	347.8 ± 131.5	0.56 ± 0.13	424.6 ± 126.5	1482.7 ± 122.7	0.3 ± 0.13

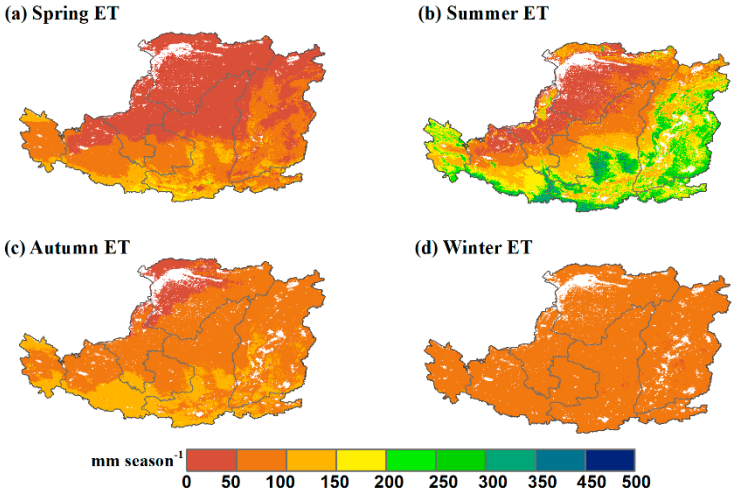

Figure 3. Spatial patterns of (**a**) spring ET, (**b**) summer ET, (**c**) autumn ET, and (**d**) winter ET averaged over 2000–2014 in the Chinese Loess Plateau.

3.2. Interannual Variability of ET in the CLP

Annual ET significantly increased across 18% of the whole CLP region during 2000–2014 (p-value < 0.05, Figure 4a1 and Table 2); of these, 71% were accompanied with positive *P* and negative AED trends (i.e., pixels of "ET+ P+ AED–" in Figure 4b1, Table 3), and 28% were accompanied with both increasing trends in *P* and AED (i.e., pixels of "ET+ P+ AED+" in Figure 4b1, Table 3). There were also 6.6% of the whole CLP area exhibiting significant declines in annual ET during the study period (Table 2). The total ET amount over active growing season and summer both significantly increased across 41% and 46.7% of the CLP area, respectively (p-value < 0.05, Table 2), and about 80% of these areas were accompanied with positive *P* and negative AED trends for both active growing season and summer (Figure 4b2,b4, Table 3). Figure 4 also shows significant declines in winter-ET for 69.4% of the CLP region (p-value < 0.05, Table 2), and quite stable spring and autumn ET values for the majority of the CLP area during 2000–2014 (Table 2).

The interannual variability of ET values averaged across the entire CLP area at different timeframes are shown in Figures 5 and 6. Results showed significant increasing trends in the ET amounts over active growing season and summer, and a decreasing trend in winter ET (p-value < 0.05, Figures 5a2 and 6a2,a4). The spatial-average ET of annual, spring, and autumn remained stable with no significant change (Figures 5a and 6a). The same variation trends were also observed for the interannual variability of ET values averaged across the main areas implemented with the GFG project (ET_{gfg}) versus other CLP areas not implemented with the GFG project (ET_{ngfg}) at different timeframes (Figures 5a and 6a). Figures 5b and 6b also show significant increases in NDVI and non-significant variations in *P* and AED during the study period in the CLP.

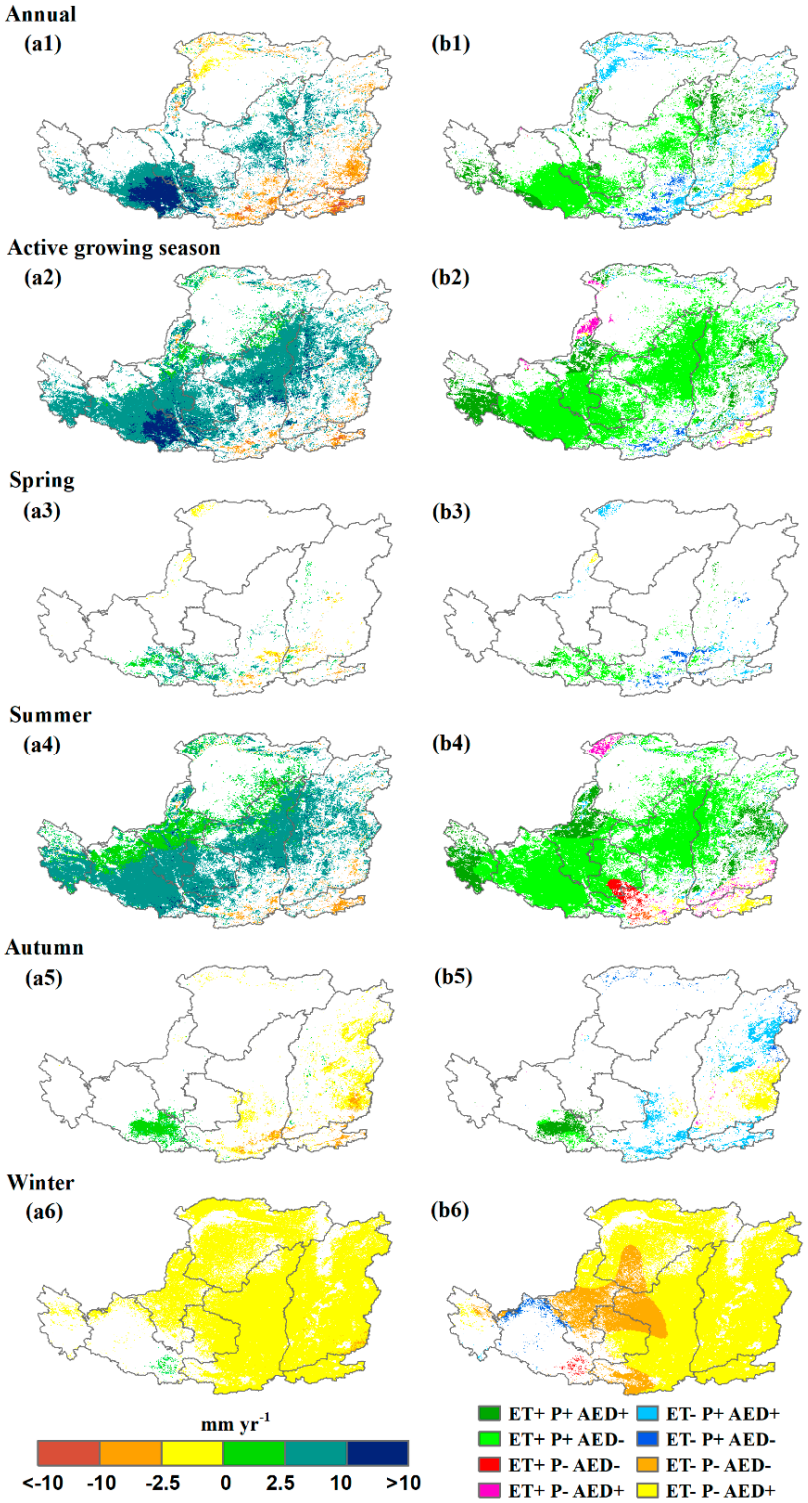

Figure 4. Spatial distributions of (**a**) ET trends and (**b**) synthetic variation signs of ET, *P,* and AED at the timescales of (1) annual, (2) active growing season, (3) spring, (4) summer, (5) autumn, and (6) winter during the time period from 2000 to 2014. Symbols "+" and "–" in the right legend indicate increasing and decreasing trends, respectively. This figure only shows pixels with significant ET trends (p-value < 0.05).

Table 2. Proportions of areas with interannual trends significantly increased or decreased in ET, *P*, AED, and NDVI (*p*-value < 0.05), and spatial-average ET trends (mm yr^{-1}) for different timescales across the CLP region during 2000–2014.

	ET		*P*		AED		NDVI		Spatial-Average ET Trend
	Increase	Decrease	Increase	Decrease	Increase	Decrease	Increase	Decrease	Trend (*p*-value)
Annual	18.0%	6.6%	6.6%	0	5.2%	0	80.0%	1.0%	1.31 (0.37)
Active growing season	41.1%	2.1%	13.3%	0	2.8%	1.5%	78.0%	0.9%	3.00 (<0.05)
Spring	2.8%	1.4%	17.6%	0	2.2%	0	64.0%	1.9%	0.21 (0.78)
Summer	46.7%	2.1%	0	0.9%	3.6%	1.2%	74.5%	0.7%	2.34 (<0.05)
Autumn	2.3%	6.2%	0	0	0.02%	0	68.6%	0.7%	−0.38 (0.43)
Winter	0.2%	69.4%	0	19.2%	1.4%	0	62.1%	1.5%	−0.87 (<0.01)

Table 3. Proportions of areas showing different variation signs of ET, *P*, and AED at different timescales in the CLP during 2000–2014. Symbols "+" and "−" indicate increasing and decreasing trends in Figure 4b, respectively.

Trend Sign	Year	Active Growing Season	Spring	Summer	Autumn	Winter
ET+ *P*+ AED+	20.7%	15.9%	12.2%	17.0%	20.1%	0
ET+ *P*+ AED−	52.2%	77.4%	55.0%	74.4%	6.6%	0
ET+ *P*− AED−	0.01%	0.01%	0	2.1%	0	0.3%
ET+ *P*− AED+	0.2%	1.6%	0.04%	2.1%	0.6%	0.01%
ET− *P*+ AED+	14.2%	1.6%	12.0%	0.9%	40.8%	0.04%
ET− *P*+ AED−	5.3%	2.1%	19.2%	0.7%	4.9%	1.1%
ET− *P*− AED−	0	0	0	0.4%	0.1%	18.6%
ET− *P*− AED+	7.4%	1.3%	1.6%	2.4%	26.9%	79.9%

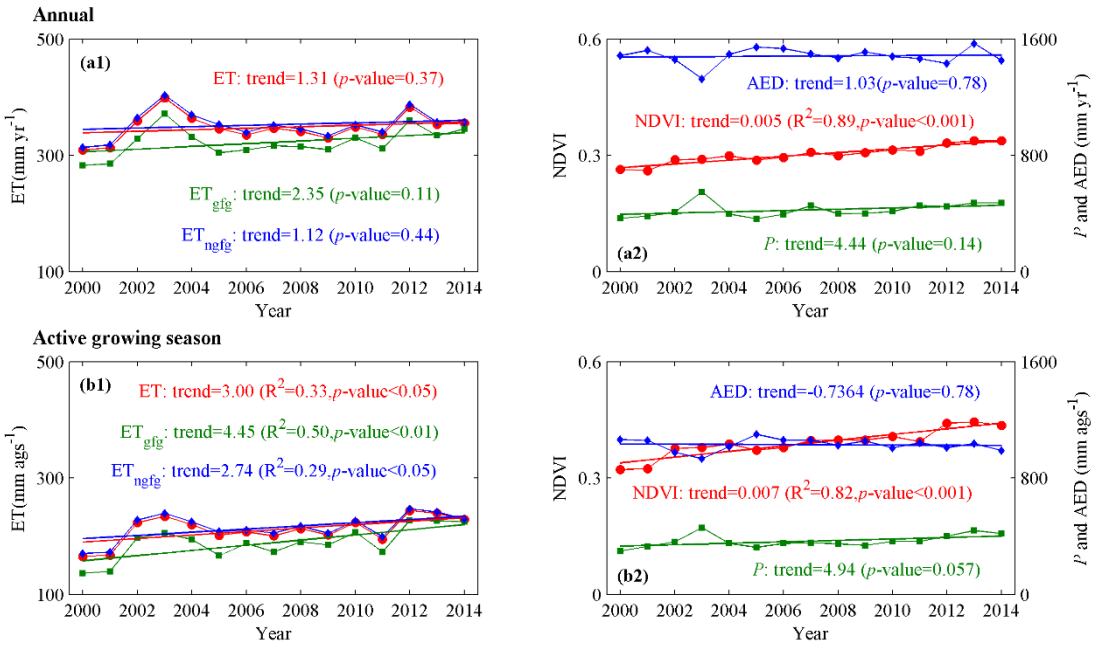

Figure 5. Interannual variability of (**a1**) annual ET and (**a2**) ET over active growing season across the entire CLP, along with main areas implemented with the GFG project (ET_{gfg}) versus other CLP areas not implemented with the GFG project (ET_{ngfg}) during 2000–2014 at the spatial-average level. The interannual variabilities of NDVI, *P*, and AED at the timescales of (**b1**) annual and (**b2**) active growing season across the entire CLP are also shown for reference. The broken lines with colors of red, green, and blue in the left panels show the interannual variability of ET across the entire CLP (denoted as ET), ET_{gfg}, and ET_{ngfg}, respectively, with annual trends (mm yr^{-1}) indicated by the texts in the same color. The broken lines and texts with colors of red, green, and blue in the right panels show the interannual variability and annual trends of NDVI, *P*, and AED, respectively.

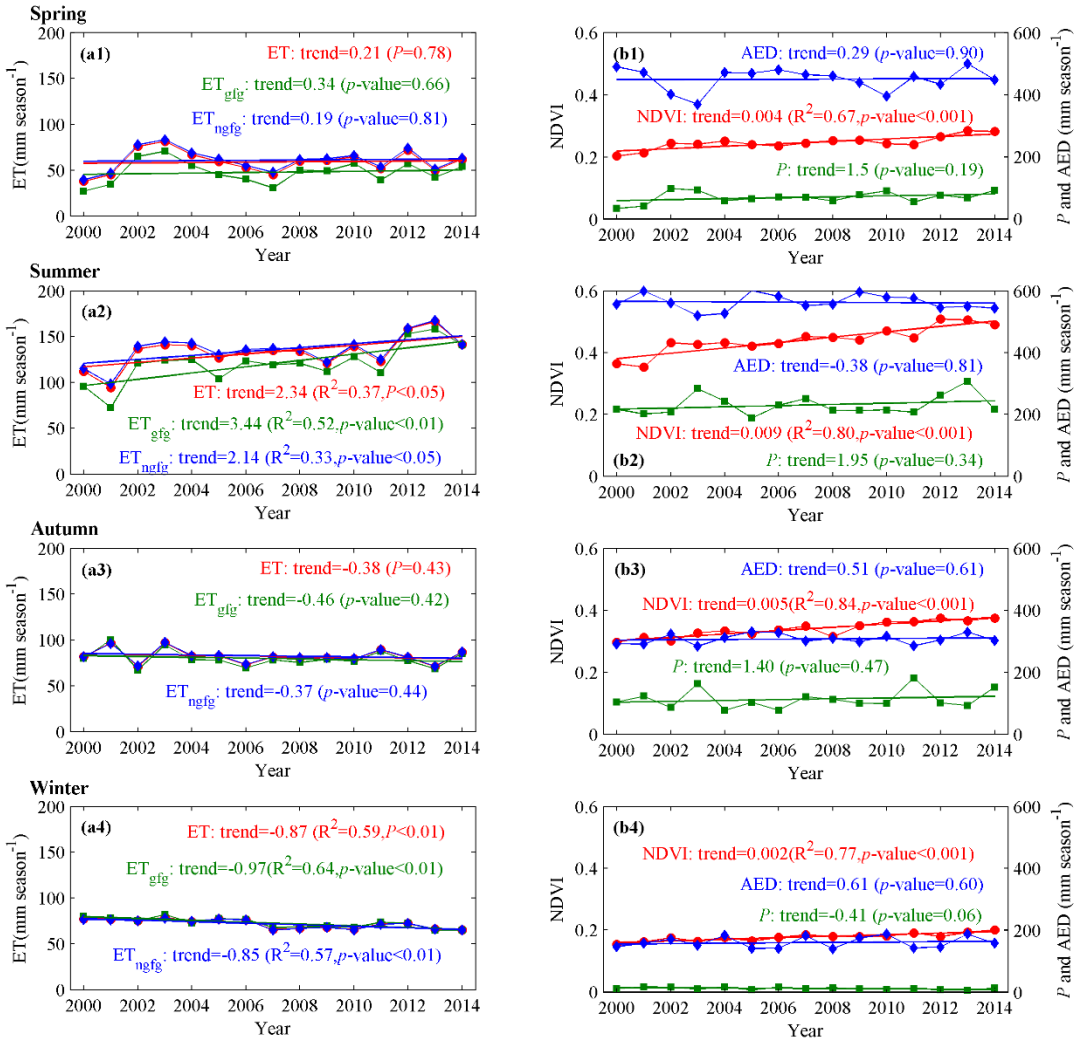

Figure 6. Interannual variability of (**a1**) spring-ET, (**a2**) summer-ET, (**a3**) autumn-ET, and (**a4**) winter-ET across the entire CLP, along with main areas implemented with the GFG project (ET_{gfg}) versus other CLP areas not implemented with the GFG project (ET_{ngfg}) during 2000–2014 at the spatial-average level. The interannual variabilities of NDVI, *P*, and AED in (**b1**) spring, (**b2**) summer, (**b3**) autumn, and (**b4**) winter across the entire CLP are also shown for reference. The broken lines with colors of red, green, and blue in the left panels show the interannual variability of ET across the entire CLP (denoted as ET), ET_{gfg}, and ET_{ngfg} for different seasons, respectively, with annual trends (mm yr^{-1}) indicated by the texts in the same color. The broken lines and texts with colors of red, green, and blue in the right panels show the interannual variability and annual trends of NDVI, *P*, and AED, respectively.

3.3. Relationships of ET Trends with Precipitation, AED, and NDVI Trends

Spatial distributions of correlation coefficients (*R*) between the detrended series of ET and *P*, AED, and NDVI are shown in Figure 7. The interannual variability of ET positively correlated with that of *P* for the majority of the CLP area (i.e., 97% on average) for annual, active growing season, and different seasons except winter, with *R* values larger than 0.5 across about 65% (61–72%) of the whole CLP area and higher *R* values for the arid and semi-arid areas (Figure 7a). For the winter, the interannual variability of winter ET was negatively but weakly correlated with that of winter *P* in 63% of the CLP area ($R > -0.5$, Figure 7a6). Figure 7 also showed negative correlations between ET and AED over more than 96% of the CLP area for annual, active growing season, and different seasons, with strong correlations ($R < -0.5$) across ~71% (43–88%) of the CLP region (Figure 7b). In contrast, the per-pixel relationships between interannual trends of ET and NDVI were positive in 81–98% of the entire CLP

area for annual, active growing season, and different seasons except winter, but weakly negative for the winter season in ~60% of the CLP region (Figure 7c).

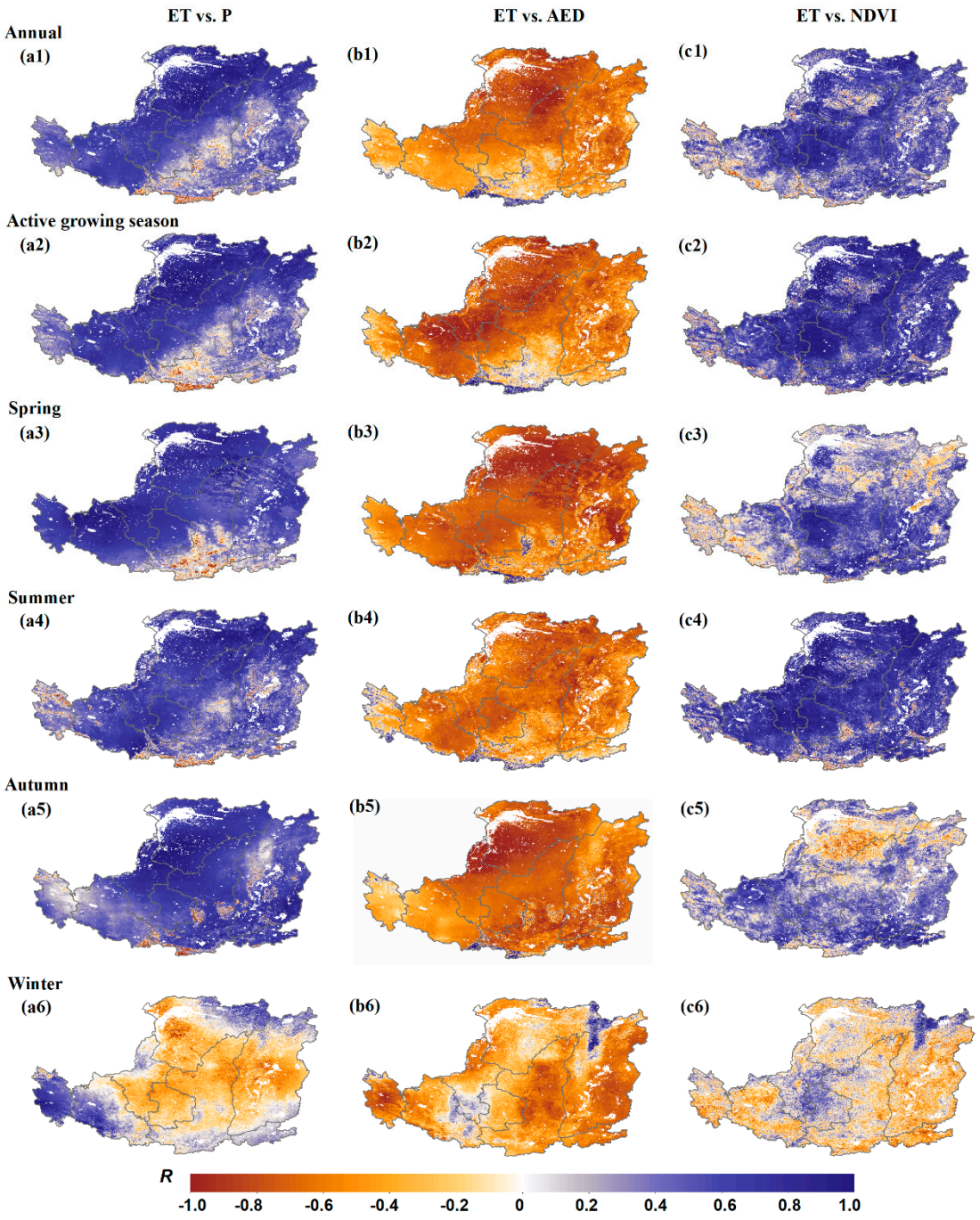

Figure 7. Spatial distributions of correlation coefficients (*R*) between (**a**) precipitation (*P*), (**b**) AED, (**c**) NDVI, and ET during 2000–2014 at the timescales of (1) annual, (2) active growing season, (3) spring, (4) summer, (5) autumn, and (6) winter across the entire CLP.

4. Discussion

4.1. Spatial Variation in CLP Ecosystem ET

Ecosystem ET is an important ecological indicator characterizing water consumption of terrestrial ecosystems [35,36]. The spatial distribution of ET was analyzed among different vegetation zones in

the CLP in this study. Results indicated that mean annual ET was generally higher for the more humid and warmer areas across the study area (Figure 2 and Table 1), which agreed with the spatial pattern of ET among different ecosystem types [6] and at the global and China-regional scales [1,37].

Spatial variation in the CLP ET was regulated by the spatial distributions of climate and vegetation conditions [1]. Previous studies demonstrated that the climatic controls on the spatial variation in ET mainly reflected in the positive effects of water supply and atmospheric evaporative demand [1,38,39]. The per-pixel ratio of annual AED to annual precipitation was always larger than 1 in the CLP (Figures 1b and 2d). It indicates that the water supply condition (i.e., precipitation) is the main climate factor controlling the spatial patterns of ET in the CLP, rather than AED [40,41], which could be also proved by the similar spatial patterns of ET and *P* in the CLP (Figures 1b and 2a). The spatial distribution of *P* in the CLP was the most important factor shaping the vegetation patterns in the CLP [42], which contributes to the higher ET values in the southeastern CLP areas. It is because that the forest vegetation, mainly growing in the southeastern CLP region (Figure 1), could better use the ground water and solar radiation because of deeper root, higher root surfaces, and denser canopies as compared to steppe vegetations [23,43]. The topography could also affect the spatial patterns of ET by transporting water from the areas with higher elevations to the southeastern areas with lower elevations in the CLP (Figure 1a) [6].

We also found that the ratio of ET over active growing season to annual ET (AGS-ET/annual ET ratio) decreased from the southeastern humid areas to the northwestern areas in the CLP (Figure 2b and Table 1). Quite low AGS-ET/annual ET ratios in the arid and semi-arid areas were related to the physiological regulation mechanisms of plants. That is, the plants in the arid areas will decrease the plant stomatal conductance in order to reduce ecosystem water loss under the environmental conditions of high AED and rare precipitation amount during active growing season [43,44].

4.2. Dominant Factors Driving Interannual Variability of ET in the CLP

The interannual variability of ET in the CLP derived from the MODIS ET dataset and its relationships with that of *P*, AED, and NDVI were analyzed at the timescales of annual, active growing season, and different seasons during the time period from 2000 to 2014. Our results manifested that the interannual trends in ET were the same in direction with *P* trends but were opposite in direction to AED trends for most areas in the CLP (with or without significant changes) at different timeframes (Figure 4 and Table 3). It suggests that the interannual variations in the CLP ET during 2000–2014 were mainly water-limited, rather than energy-limited, from the perspective of water- and energy-limited evaporation [32,45]. Our results also indicated strongly positive relationships between the interannual trends of ET and NDVI for the majority of CLP areas at different timescales except winter (Figure 7c). Previous studies showed that increasing vegetation coverage acts to promote the proportions of vegetation transpiration and evaporation of canopy interception, but decrease soil evaporation [3,37,46], which indicated that vegetation coverage change (measured by NDVI change in this study) could affect the ET variation through altering the interannual variations in the different components of ecosystem ET [1].

In this study, ecosystem ET varied with temporal variations in the climate and vegetation factors in the CLP, but with different dominant factor(s) in different seasons for different areas during 2000–2014. Summer ET and ET over active growing season significantly increased for more than 40% of the whole CLP area (Table 2), primarily distributing in the forest-steppe and steppe zones (Figure 4a2,a4). It should primarily be attributed to the pronounced increases in summer NDVI in these areas (Figure S4c4), mainly due to the intensive revegetation (i.e., the GFG project) implemented in these areas [23]. The positive correlations between interannual variabilities of ET and NDVI were much stronger in summer as compared to other seasons (Figure 7c), suggesting that NDVI regulations on the ET variations were dominant by increasing vegetation transpiration and evaporation of canopy interception. The non-significantly increasing summer precipitation could also promote the summer-ET in these areas because of relatively higher AED in summer (Figure 6b2). Therefore, the pronounced

increases in the vegetation coverage (NDVI) together with non-significant increasing precipitation in summer led to significantly increased ET in summer and active growing season for most areas and the spatial-average level across the CLP area over the study period.

As to ET trends in spring and autumn, this study indicated that NDVI also significantly increased in spring and autumn for most areas in the CLP (Figure S4c3,c5). But the corresponding relationships between interannual variabilities of NDVI and ET were much weaker in spring and autumn, and spring and autumn ET remained quite stable for the majority of the CLP area during 2000–2014 (Table 2). It might be explained by the decreased soil evaporation at higher NDVI [3,46], which could offset the increases in the total ET amounts in spring and summer to some extent [23,43]. Spring and autumn ET also significantly decreased in some areas of the southeastern CLP region during 2000–2014 (Figure 4a3,a5), which was mainly caused by the increasing precipitation in these areas (i.e., manifested as "ET–P+AED+/–" in Figure 4b3,b5, Table 3). This is because plant growth might be limited to some extent due to the increased cloudy days (related with increasing precipitation events) and relatively lower air temperature in spring and autumn, which was proved by the negative relationships between the interannual trends of ET and precipitation in spring and autumn in the southeastern CLP areas (Figure 7a3).

We also found that winter ET decreased significantly in most areas of the CLP region during 2000–2014 (Figure 4a6), and ET variations were weakly correlated with either the decreasing precipitation or the increasing NDVI in winter (Figure 7a6,c6). In addition, the precipitation amounts were consistently lower than the ET amounts in winter (Figure 6a4,b4). It might be explained by the effects of soil freezing–thawing processes and snow sublimation on the winter ET. A previous study demonstrated that there exist several soil freezing–thawing cycles from late November to early March in arid regions of China, which could significantly affect land surface heat and water balance [47]. That is, ecosystem ET should be very small during the freezing periods due to the relatively less liquid soil moisture, and higher during the thawing periods [47]. The ET over snow surface (i.e., snow sublimation) has been proved be positively correlated with air temperature [48]. Since the air temperature of winter decreased in 94% of the entire CLP area during 2000–2014 [23], the soil freezing status and snow sublimation would be lengthened or strengthened as a result, hence contributing to decreases in winter-ET.

As discussed above, the ET variations over different seasons were regulated with different factors for different areas, and their combined effects finally led to the interannual variability of annual total ET amounts (Figure 4a1). Feng et al. [11] has concluded that the interannual variability of annual ET was mainly controlled by revegetation programs in the CLP, rather than climate changes during 2000–2010 using MODIS ET dataset and ecosystem models. In our study here, we found that the climate changes (i.e., precipitation and temperature changes) were also important factors controlling ET variations in different seasons, especially in winter. For example, the areas without the GFG project in the southwestern CLP region showed significant increases in the summer ET and, hence, annual ET (Figure 4a1,a4). Also, the ET variation trends were exactly consistent for the entire CLP region, the main areas implemented with the GFG project, and other CLP areas not implemented with GFG project at different timeframes (Figures 5a and 6a). It means that climate change has played an essential role in shaping the temporal variations in the CLP ET. It is necessary to quantify the effects of climate changes and vegetation coverage changes on ET variations using modelling techniques in the future, if a deeper understanding of the temporal variations in the CLP ET and its underlying mechanisms is to be achieved.

4.3. Uncertainties

The spatiotemporal patterns of ET in response to climate and vegetation coverage changes across the CLP region were examined mainly based on the MODIS ET dataset (MOD16), and gridded meteorological data interpolated with ground-based meteorological observations using the AUSPLINE software. Although the MODIS ET data were validated with acceptable performance in generating

site-level ET measurements (Figure S2), some caution should be observed as there may be uncertainties in the algorithm and input variables applied in producing MODIS ET data, especially the biome information derived from remote-sensing products (e.g., leaf area index and land cover type). The spatial resolution of 1 km^2 for land cover information seems also to be quite coarse as compared to the fragmentized landforms in the CLP. Future improvements in the accuracy of land cover products could largely enhance the accuracy in the ET-related analyses in the CLP.

Uncertainties in the gridded meteorological datasets used in the MOD16 algorithm (i.e., GMAO reanalysis data) and spatial relationship analyses in this study (i.e., AUSPLINE-interpolated data) could also cause some uncertainties. Good performance has been observed for both the GMAO and AUSPLINE-interpolated P and T_a datasets when compared with point-scale measurements in China (Figure S3). Although the data source for T_a data was not consistent for the MOD16 algorithm and AED calculation in this study, it was confirmed that the gridded T_a dataset from the AUSPLINE software was closely correlated with the GMAO reanalysis data (0.5° × 0.625°, v. 5.12.4), with R^2 and RMSE of 0.92 and 1.8 °C, respectively (Figure S3), which demonstrates small uncertainties brought by different T_a data in this study.

5. Conclusions

Spatiotemporal variations in ecosystem ET and its relationships with regional climate variability and vegetation coverage changes were investigated at the timescales of annual, active growing season, and different seasons across the entire CLP from 2000 to 2014, mainly based on a MODIS ET dataset. Our results showed that mean annual ET varied distinctly among different vegetation zones, with an overall mean of 347.8 ± 131.5 mm yr^{-1}, and generally higher for the humid areas. Our findings also showed that ET variation trends were exactly consistent for the entire CLP region, the areas mainly implemented with the GFG project, and other CLP areas not implemented with GFG project at different timescales during 2000–2014. Climatic controls on the ET variation in the CLP were mainly water-limited, while vegetation controls on the ET variation were mainly accomplished through altering the variation trends of different components of ecosystem ET (i.e., increasing NDVI acts to promote the proportions of vegetation transpiration and evaporation of canopy interception, but decrease soil evaporation). Our results demonstrated that climate change played an essential role in shaping the temporal variations in the CLP ET, and it is necessary to quantify the effects of climate changes and vegetation coverage changes on ET variations using modelling techniques in the future. As a typical water-limited region undergoing climate change and large-scale revegetation, our analyses on the ET variations will enhance our understanding on the water consumption and water allocation of terrestrial ecosystems in other regions with similar characteristics.

Supplementary Materials: The following is available online at http://www.mdpi.com/2073-4441/11/8/1625/s1, Figure S1: Eddy-covariance flux sites in China used for validating MODIS ET dataset and gridded P and T_a datasets generated by AUSPLINE software in this study. Figure S2: Comparison between eddy-covariance ET and MODIS ET at annual scale in China and monthly scale in the Chinese Loess Plateau. Figure S3: Comparison between point-scale T_a and P observations and interpolated data from AUSPLINE software and GMAO reanalysis data. Figure S4: Spatial patterns of precipitation trends, atmospheric evaporative demand trends, and NDVI trends during 2000–2014 at different timescales in the Chinese Loess Plateau.

Author Contributions: H.Z. performed the data collection, data processing, and manuscript preparation. H.L. and X.Z. helped the data analysis. All authors participated in the revision of the manuscript.

Funding: This research was jointly funded by National Natural Science Foundation of China (grant nos. 31700414, 31500390, 41790444) and Strategic Priority Research Program of the Chinese Academy of Sciences (grant no. XDA19020302).

Acknowledgments: We acknowledge the database and technical support from the China Meteorological Data Service Center for providing point-scale meteorological data, and ChinaFLUX for providing eddy-covariance ET data and auxiliary air temperature and precipitation data for validation. We thank the editors and anonymous reviewers for their constructive comments that helped improve this paper.

Conflicts of Interest: The authors declare no conflict of interest.

References

1. Zheng, H.; Yu, G.; Wang, Q.; Zhu, X.; He, H.; Wang, Y.; Zhang, J.; Li, Y.; Zhao, L.; Zhao, F. Spatial variation in annual actual evapotranspiration of terrestrial ecosystems in China: Results from eddy covariance measurements. *J. Geogr. Sci.* **2016**, *26*, 1391–1411. [CrossRef]
2. Wang, K.C.; Dickinson, R.E. A review of global terrestrial evapotranspiration: Observation, modeling, climatology, and climatic variability. *Rev. Geophys.* **2012**, *50*, RG2005. [CrossRef]
3. Hu, Z.; Yu, G.; Fu, Y.; Sun, X.; Li, Y.; Shi, P.; Wang, Y.; Zheng, Z. Effects of vegetation control on ecosystem water use efficiency within and among four grassland ecosystems in China. *Glob. Chang. Biol.* **2008**, *14*, 1609–1619. [CrossRef]
4. Oki, T.; Kanae, S. Global hydrological cycles and world water resources. *Science* **2006**, *313*, 1068–1072. [CrossRef] [PubMed]
5. World Meteorological Organization (WMO) Geneva. *Guide to Hydrological Practices: Volume I Hydrology—From Measurement to Hydrological Information*, 6th ed.; WMO Technical Publication No 168; World Meteorological Organization (WMO) Geneva: Geneva, Switzerland, 2008.
6. Li, H.; Wang, A.; Yuan, F.; Guan, D.; Jin, C.; Wu, J.; Zhao, T. Evapotranspiration dynamics over a temperate meadow ecosystem in eastern Inner Mongolia, China. *Environ. Earth Sci.* **2016**, *75*, 978. [CrossRef]
7. Liu, S.; Xu, Z.; Song, L.; Zhao, Q.; Ge, Y.; Xu, T.; Ma, Y.; Zhu, Z.; Jia, Z.; Zhang, F. Upscaling evapotranspiration measurements from multi-site to the satellite pixel scale over heterogeneous land surfaces. *Agric. For. Meteorol.* **2016**, *230–231*, 97–113. [CrossRef]
8. Ren, C.F.; Li, Z.H.; Zhang, H.B. Integrated multi-objective stochastic fuzzy programming and AHP method for agricultural water and land optimization allocation under multiple uncertainties. *J. Clean. Prod.* **2019**, *210*, 12–24. [CrossRef]
9. Fu, B.; Wang, S.; Liu, Y.; Liu, J.; Liang, W.; Miao, C. Hydrogeomorphic Ecosystem Responses to Natural and Anthropogenic Changes in the Loess Plateau of China. *Annu. Rev. Earth Planet. Sci.* **2017**, *45*, 223–243. [CrossRef]
10. Chen, Y.; Wang, K.; Lin, Y.; Shi, W.; Song, Y.; He, X. Balancing green and grain trade. *Nat. Geosci.* **2015**, *8*, 739–741. [CrossRef]
11. Feng, X.; Fu, B.; Piao, S.; Wang, S.; Ciais, P.; Zeng, Z.; Lü, Y.; Zeng, Y.; Li, Y.; Jiang, X.; et al. Revegetation in China's Loess Plateau is approaching sustainable water resource limits. *Nat. Clim. Chang.* **2016**, *6*, 1019–1022. [CrossRef]
12. Jia, X.; Shao, M.a.; Zhu, Y.; Luo, Y. Soil moisture decline due to afforestation across the Loess Plateau, China. *J. Hydrol.* **2017**, *546*, 113–122. [CrossRef]
13. Feng, X.M.; Sun, G.; Fu, B.J.; Su, C.H.; Liu, Y.; Lamparski, H. Regional effects of vegetation restoration on water yield across the Loess Plateau, China. *Hydrol. Earth Syst. Sci.* **2012**, *16*, 2617–2628. [CrossRef]
14. Wang, Y.; Shao, M.; Zhu, Y.; Liu, Z. Impacts of land use and plant characteristics on dried soil layers in different climatic regions on the Loess Plateau of China. *Agric. For. Meteorol.* **2011**, *151*, 437–448. [CrossRef]
15. Li, Y.; Liu, C.; Zhang, D.; Liang, K.; Li, X.; Dong, G. Reduced Runoff Due to Anthropogenic Intervention in the Loess Plateau, China. *Water* **2016**, *8*, 458. [CrossRef]
16. Mu, Q.; Heinsch, F.A.; Zhao, M.; Running, S.W. Development of a global evapotranspiration algorithm based on MODIS and global meteorology data. *Remote Sens. Environ.* **2007**, *111*, 519–536. [CrossRef]
17. Sun, Y.; Piao, S.; Huang, M.; Ciais, P.; Zeng, Z.; Cheng, L.; Li, X.; Zhang, X.; Mao, J.; Peng, S.; et al. Global patterns and climate drivers of water-use efficiency in terrestrial ecosystems deduced from satellite-based datasets and carbon cycle models. *Glob. Ecol. Biogeogr.* **2016**, *25*, 311–323. [CrossRef]
18. Hu, Z.; Wu, G.; Zhang, L.; Li, S.; Zhu, X.; Zheng, H.; Zhang, L.; Sun, X.; Yu, G. Modeling and Partitioning of Regional Evapotranspiration Using a Satellite-Driven Water-Carbon Coupling Model. *Remote Sens.* **2017**, *9*, 54. [CrossRef]
19. Ivezic, V.; Bekic, D.; Horvat, B. Modelling of Basin Wide Daily Evapotranspiration with a Partial Integration of Remote Sensing Data. *Atmosphere* **2018**, *9*, 120. [CrossRef]
20. Bi, Y.; Qiu, L.; Zhakypbek, Y.; Jiang, B.; Cai, Y.; Sun, H. Combination of plastic film mulching and AMF inoculation promotes maize growth, yield and water use efficiency in the semiarid region of Northwest China. *Agric. Water Manag.* **2018**, *201*, 278–286. [CrossRef]

21. Cai, T.; Zhang, C.; Huang, Y.; Huang, H.; Yang, B.; Zhao, Z.; Zhang, J.; Jia, Z. Effects of different straw mulch modes on soil water storage and water use efficiency of spring maize (Zea mays L.) in the Loess Plateau of China. *Plant. Soil Environ.* **2016**, *61*, 253–259. [CrossRef]
22. Allen, R. Why do we care about ET? *Southwest Hydrol.* **2008**, *7*, 18–19.
23. Zheng, H.; Lin, H.; Zhou, W.; Bao, H.; Zhu, X.; Jin, Z.; Song, Y.; Wang, Y.; Liu, W.; Tang, Y. Revegetation has increased ecosystem water-use efficiency during 2000–2014 in the Chinese Loess Plateau: Evidence from satellite data. *Ecol. Indic.* **2019**, *102*, 507–518. [CrossRef]
24. Baldocchi, D. 'Breathing' of the terrestrial biosphere: Lessons learned from a global network of carbon dioxide flux measurement systems. *Aust. J. Bot.* **2008**, *56*, 1–26. [CrossRef]
25. Yu, G.R.; Fu, Y.L.; Sun, X.M.; Wen, X.F.; Zhang, L. Recent progress and future directions of ChinaFLUX. *Sci. China Ser. D Earth Sci.* **2006**, *49*, 1–23. [CrossRef]
26. Zhang, T.; Peng, J.; Liang, W.; Yang, Y.; Liu, Y. Spatial-temporal patterns of water use efficiency and climate controls in China's Loess Plateau during 2000–2010. *Sci. Total Environ.* **2016**, *565*, 105–122. [CrossRef] [PubMed]
27. Mu, Q.; Zhao, M.; Running, S.W. Improvements to a MODIS global terrestrial evapotranspiration algorithm. *Remote Sens. Environ.* **2011**, *115*, 1781–1800. [CrossRef]
28. Xiao, J.; Sun, G.; Chen, J.; Chen, H.; Chen, S.; Dong, G.; Gao, S.; Guo, H.; Guo, J.; Han, S. Carbon fluxes, evapotranspiration, and water use efficiency of terrestrial ecosystems in China. *Agric. For. Meteorol.* **2013**, *182*, 76–90. [CrossRef]
29. Liu, X.; Zhang, N.; Lan, H.X. Effects of sand and water contents on the small-strain shear modulus of loess. *Eng. Geol.* **2019**, *260*, 105202. [CrossRef]
30. Zheng, H.; Yu, G.; Zhu, X.; Wang, Q.; Zhang, L.; Chen, Z.; Sun, X.; He, H.; Su, W.; Wang, Y.; et al. A dataset of actual evapotranspiration and water use efficiency of typical terrestrial ecosystems in China (2000–2010). *China Sci. Data* **2019**, *4*. [CrossRef]
31. Hutchinson, M. Interpolating mean rainfall using thin plate smoothing splines. *Int. J. Geogr. Inf. Syst.* **1995**, *9*, 385–403. [CrossRef]
32. Zheng, H.; Yu, G.; Wang, Q.; Zhu, X.; Yan, J.; Wang, H.; Shi, P.; Zhao, F.; Li, Y.; Zhao, L. Assessing the ability of potential evapotranspiration models in capturing dynamics of evaporative demand across various biomes and climatic regimes with ChinaFLUX measurements. *J. Hydrol.* **2017**, *551*, 70–80. [CrossRef]
33. Linacre, E.T. A simple formula for estimating evaporation rates in various climates, using temperature data alone. *Agric. Meteorol.* **1977**, *18*, 409–424. [CrossRef]
34. Allen, R.G.; Pereira, L.S.; Raes, D.; Smith, M. *Crop Evapotranspiration—Guidelines for Computing Crop Water Requirements, FAO Irrigation and Drainage Paper No. 56*; FAO: Rome, Italy, 1998.
35. Zheng, H.; Wang, Q.F.; Zhu, X.J.; Li, Y.N.; Yu, G.R. Hysteresis Responses of Evapotranspiration to Meteorological Factors at a Diel Timescale: Patterns and Causes. *PLoS ONE* **2014**, *9*, e98857. [CrossRef] [PubMed]
36. Zhu, X.J.; Yu, G.R.; Hu, Z.M.; Wang, Q.F.; He, H.L.; Yan, J.H.; Wang, H.M.; Zhang, J.H. Spatiotemporal variations of T/ET (The ratio of transpiration to evapotranspiration) in three forests of Eastern China. *Ecol. Indic.* **2015**, *52*, 411–421. [CrossRef]
37. Jung, M.; Reichstein, M.; Margolis, H.A.; Cescatti, A.; Richardson, A.D.; Arain, M.A.; Arneth, A.; Bernhofer, C.; Bonal, D.; Chen, J.; et al. Global patterns of land-atmosphere fluxes of carbon dioxide, latent heat, and sensible heat derived from eddy covariance, satellite, and meteorological observations. *J. Geophys. Res.* **2011**, *116*, G00J07. [CrossRef]
38. Budyko, M. *Climate and Life, Translated from Russian by DH Miller*; Academic Press: San Diego, CA, USA, 1974.
39. Yang, D.; Sun, F.; Liu, Z.; Cong, Z.; Ni, G.; Lei, Z. Analyzing spatial and temporal variability of annual water-energy balance in nonhumid regions of China using the Budyko hypothesis. *Water Resour. Res.* **2007**, *43*, W04426. [CrossRef]
40. Dai, A.; Trenberth, K.E.; Qian, T. A global dataset of Palmer Drought Severity Index for 1870–2002: Relationship with soil moisture and effects of surface warming. *J. Hydrometeorol.* **2004**, *5*, 1117–1130. [CrossRef]
41. Donohue, R.J.; McVicar, T.R.; Roderick, M.L. Assessing the ability of potential evaporation formulations to capture the dynamics in evaporative demand within a changing climate. *J. Hydrol.* **2010**, *386*, 186–197. [CrossRef]

42. Zheng, H.; Lin, H.; Zhu, X.; Jin, Z.; Bao, H. Divergent spatial responses of plant and ecosystem water-use efficiency to climate and vegetation gradients in the Chinese Loess Plateau. *Glob. Planet. Chang.* **2019**, *181*, 102995. [CrossRef]
43. Niu, S.L.; Xing, X.R.; Zhang, Z.; Xia, J.Y.; Zhou, X.H.; Song, B.; Li, L.H.; Wan, S.Q. Water-use efficiency in response to climate change: From leaf to ecosystem in a temperate steppe. *Glob. Chang. Biol.* **2011**, *17*, 1073–1082. [CrossRef]
44. Farquhar, G.D.; Sharkey, T.D. Stomatal conductance and photosynthesis. *Annu. Rev. Plant. Physiol.* **1982**, *33*, 317–345. [CrossRef]
45. McVicar, T.R.; Roderick, M.L.; Donohue, R.J.; Li, L.T.; Van Niel, T.G.; Thomas, A.; Grieser, J.; Jhajharia, D.; Himri, Y.; Mahowald, N.M.; et al. Global review and synthesis of trends in observed terrestrial near-surface wind speeds: Implications for evaporation. *J. Hydrol.* **2012**, *416–417*, 182–205. [CrossRef]
46. Law, B.; Falge, E.; Gu, L.; Baldocchi, D.; Bakwin, P.; Berbigier, P.; Davis, K.; Dolman, A.; Falk, M.; Fuentes, J. Environmental controls over carbon dioxide and water vapor exchange of terrestrial vegetation. *Agric. For. Meteorol.* **2002**, *113*, 97–120. [CrossRef]
47. Zhang, Z.; Wang, W.; Gong, C.; Wang, Z.; Duan, L.; Yeh, T.c.J.; Yu, P. Evaporation from seasonally frozen bare and vegetated ground at various groundwater table depths in the Ordos Basin, Northwest China. *Hydrol. Process.* **2019**, *33*, 1338–1348. [CrossRef]
48. Li, H.; Wang, A.; Guan, D.; Jin, C.; Wu, J.; Yuan, F.; Shi, T. Empirical Model Development for Ground Snow Sublimation beneath a Temperate Mixed Forest in Changbai Mountain. *J. Hydrol. Eng.* **2016**, *21*, 04016040. [CrossRef]